EARTH SCIENCES
RESEARCH JOURNAL
Earth Sci. Res. J. Vol. 29, No. 2 (June, 2025): 139 -148

UNIVERSIDAD NACIONAL DE COLOMBIA

GEOLOGY

Mineralogical Characteristics and Colouring Mechanism of Hydrothermal Fluorite in the Sumochagan Obo Deposit, Inner Mongolia, north China

Zeng-Qi Lu[1], Liang Zhang[1, 2]*, Zu-Yan Chen[3], Biao Jiang[4]

1 School of Gemmology, China University of Geosciences, Beijing 100083, China

2 Frontiers Science Center for Deep-time Digital Earth, State Key Laboratory of Geological Processes and Mineral Resources, China University of Geosciences, Beijing 100083, China

3 School of Earth Sciences, China University of Geosciences, Beijing 100083, China

4 Institute of Mineral Resources, Chinese Academy of Geological Sciences, Beijing 100037, China

*Corresponding author: liang.zhang@cugb.edu.cn

ABSTRACT

The Sumochagan Obo fluorite deposit, located in the northern part of Siziwangqi, Inner Mongolia, is recognized as a world-class fluorite-only deposit. However, research on the mineralogical characteristics and genesis of fluorite in this area remains relatively limited. To further elucidate the coloring and formation mechanisms of fluorite in this area, this research investigates the mineralogical and spectral characteristics of green and purple fluorite using Diamond View, infrared spectroscopy, ultraviolet-visible absorption spectroscopy, and laser Raman spectroscopy. Geochemical analysis was conducted using energy dispersive X-ray fluorescence spectrometry, wavelength dispersive X-ray fluorescence spectrometry, and inductively coupled plasma mass spectrometry (ICP-MS). In the ultraviolet-visible absorption spectrum, green fluorite samples exhibit absorption peaks at 223 nm, associated with Y and F centers. Absorption peaks at 693, 440, 360, and 276 nm are attributed to the presence of Sm^{2+}, while peaks at 587 and 591 nm are caused by calcium colloidal color centers. The purple color of fluorite is likely due to YO_2 centers, as indicated by absorption peaks at 276 and 261 nm in the ultraviolet-visible absorption spectrum of purple samples. Through the Tb/Ca-Tb/La plot, it is observed that most fluorite samples from this mining area fall within the hydrothermal field, which aligns with geological observations. The measured total rare earth elements (∑REE) of fluorite in this deposit fall between magmatic-hydrothermal fluids and meteoric water, indicating that the deposit was formed by the mixing of magmatic-hydrothermal processes with meteoric water involvement.

Keywords: Hydrothermal fluorite; Rare earth elements; Colouring mechanism; Magmatic-hydrothermal deposit; Sumochagan Obo deposit.

Características mineralógicas y mecanismo de coloración de la fluorita hidrotermal en el yacimiento Sumochagan Obo, Mongolia Interior, norte de China

RESUMEN

El depósito de fluorita de Sumochagan, localizado al norte de Siziwangqi, en la región de Mongolia interior, es reconocido como un depósito único de clase mundial. Sin embargo, la investigación de las características y origen de las fluoritas en esta área aún es relativamente limitado. Para definir los mecanismos de formación y coloración de estas fluoritas, este trabajo investiga las características espectrales y mineralógicas de fluoritas violetas y verdes a través de los métodos Diamond View, espectroscopía infrarroja, espectroscopía de absorción visible ultravioleta y espectroscopía laser Raman. Análisis geoquímicos se llevaron a cabo con el método de espectometría fluorescente de energía dispersiva de rayos X, espectometría fluorescente de ancho de onda dispersiva de rayos X y espectrometría de masas de plasma acoplado. En el espectro de absorción visible ultravioleta, las muestras de fluoritas verdes muestran picos de absorción de 223 nm, asociados con centros Y y F. Los picos de absorción a 693, 440, 360 y 276 nm se atribuyen a la presencia de Sm^{2+}, mientras que los de 587 y 591, nm son causados por centros de color coloidal de calcio. El color violeta de las fluoritas es posible que se deba a los centros de YO_2, de acuerdo con los picos de absorción de 276 y 261 nm en el espectro de absorción visible ultravioleta de las muestras violetas. En el diagrama Tb/Ca-Tb/La, se observa que la mayoría de las muestras de fluorita de esta zona minera se encuentran dentro del campo hidrotermal, lo cual concuerda con las observaciones geológicas. El total de elementos de tierras raras (∑REE) medidos en fluorita en este depósito se encuentra entre fluidos magmático-hidrotermales y agua meteórica, lo que indica que el depósito se formó mediante la mezcla de procesos magmático-hidrotermales con la participación de agua meteórica.

Palabras clave: Fluorita hidrotermal; Elementos de tierras raras; Mecanismo de coloración; Depósito magmático-hidrotermal; Depósito Sumochagan Obo.

Record
Manuscript received: 26/07/2024
Accepted for publication: 17/04/2025

How to cite this item:
Lu, Z, Q., Zhang, L., Chen, Z. Y., & Jiang, B. (2025). Mineralogical Characteristics and Colouring Mechanism of Hydrothermal Fluorite in the Sumochagan Obo Deposit, Inner Mongolia, north China. *Earth Sciences Research Journal, 29*(2),139-148. https://doi.org/10.15446/esrj.v29n2.115986

1. Introduction

Fluorite, with the main component CaF_2, is a major source of the chemical element fluorine. It belongs to the cubic crystal system, primarily exhibiting a cubic crystal habit, though octahedral and dodecahedral forms, often seen as twins, can occasionally occur. The crystal structure of fluorite is stable and impurities are not easily incorporated. The radius of the Ca ion in fluorite is similar to that of rare earth ions, facilitating isostructural substitution. Rare earth elements typically replace Ca ions with eight-coordination, entering the crystal lattice (Shannon, 1976; Boynton and Wark, 1984; Haschke et al., 2021). Due to the geochemical behavior of rare earth elements (REE) being very similar and relatively stable, later geological events rarely alter their distribution pattern in rocks and minerals. Therefore, the distribution pattern of REE in fluorite provides significant insights into its formation environment and sources (Schwinn and Markl, 2005; Alipour et al., 2014; Rezaei Azizi et al., 2018; Rezaei Azizi et al., 2020).

Hydrothermal fluorite is a product of ore-forming fluid evolution and serves as an important medium for studying the geochemical behavior of REE in hydrothermal ore-forming processes (Ding et al., 2003; Sun et al., 2008; Sun et al., 2014; Huang et al., 2015). Fluorite occurs in various colors, commonly green, purple, and blue. The coloring mechanisms can be classified into three categories: complex center coloration involving rare earth ions and/or oxygen, divalent rare earth ion coloration, and metallic calcium colloid coloration. The first category includes F centers coordinated with Y elements, coexisting F centers coordinated with Y and Ce, YO_2 centers, and O^{3-} substitution. Divalent rare earth ions manifest in ion coloration, such as Sm^{2+} and Eu^{2+} (Bill and Galas, 1978).

Fluorite has extensive applications in industries such as new energy, national defense, and medicine, making it an important strategic mineral resource. It is primarily used in the industrial manufacturing of hydrofluoric acid and as a flux in the steel industry. With advancements in modern industrial and scientific technologies, fluorite is also used in components of high-power laser devices and rocket fuels (Sun et al., 2009, 2010; Redina et al., 2020; Zhou et al., 2022). Additionally, due to its bright colors and high transparency, fluorite is used in the jewelry industry. Industrially valuable fluorite deposits are distributed in over forty countries worldwide, predominantly in the circum-Pacific metallogenic belt (Zhao et al., 2020). Compared to other regions, China's fluorite resources have unique advantages. With low impurity content, particularly low levels of phosphorus, sulfur, and arsenic, and favorable mining conditions, they have high development value and hold an important position in global fluorite resources (Zhao et al., 2020). Researchers have studied several fluorite mining areas in China, including the Xitian area in southern Guangxi (Liu et al., 2020), the Yangshan area in Luanchuan, Henan Province (Zhang et al., 2021), and the Lishan area in Pingjiang, Hunan Province (Chen et al., 2023).

The Sumochagan Obo fluorite deposit, located in the northern part of Siziwangqi, Inner Mongolia, is a world-class fluorite-only deposit. Current research on this deposit primarily focuses on its REE geochemical characteristics. The fluorite deposits in the area exhibit similar trace element characteristics, indicating a consistent ore-forming material source, with the ore-forming fluids mainly belonging to the H_2O-CO_2-NaCl system (Xu et al., 2009). Research on the gemological characteristics and coloring mechanisms of fluorite in this deposit is still lacking. This research aims to conduct a systematic analysis of the mineralogical and gemological characteristics of the fluorite through basic gemological experiments, spectroscopy, and geochemical analysis. It also seeks to conduct preliminary analyses and discussions on the mineral chemical composition and coloring mechanisms of purple and green fluorite in the deposit. Furthermore, through the trace element characteristics of fluorite, it aims to explore its ore-forming process.

2. Regional and Local Geology

The Sumochagan Obo, located in northern Inner Mongolia, is positioned in the eastern segment of the Late Paleozoic Central Asian Orogen, between the Siberian Craton and the North China Craton. It is situated between the Solon suture zone and the Hegenshan deep fault, and lies at the northeastern end of the Baiyun Obo-Erenhot rare earth, iron, gold, and fluorite metallogenic belt (Figure 1; Yu et al., 2018).

The Solon suture zone extends from Solon Obo to Linxi, consisting of a mixed rock belt composed of blueschist and serpentinite. The primary rock types include limestone, quartzite, mafic and ultramafic rocks, dolomite, and blueschist (Xu et al., 2009). The Erenhot-Hegenshan deep fault zone trends NEE-NE, extending westward into Mongolia and eastward, where it is overridden by Neogene strata. This fault zone comprises a series of thrust or imbricate faults, serpentinite melange blocks, tectonic breccia zones, and shear zones.

The Sumochagan Obo area possesses abundant fluorite deposits, primarily including the super-large Sumochagan Obo fluorite deposit and the medium-sized Aobaotu fluorite deposit. The exposed strata belong to the Lower Permian Dashizhai Formation, consisting of volcano-sedimentary rocks. The deposit is located at the outer contact zone between the volcano-sedimentary rocks of the Early Permian Dashizhai Formation and the Early Cretaceous Weijing granites. The exposed strata mainly comprise Upper Cretaceous sandstone, sand-gravel conglomerate, and locally, Jurassic-Cretaceous low-grade metamorphic rocks of the Ailegema Formation, along with volcano-sedimentary rocks of the Permian Dashizhai Formation (Xu et al., 2009). Magmatic rocks, which are well developed in the region, mainly include Early Cretaceous medium-coarse-grained porphyritic biotite granite. Regional faults primarily trend in a near north-south, north-northwest, and northeast direction (Zhang et al., 2019).

Fluorite are bodies exhibit gentle undulating shapes in both trend and dip directions, generally tilting towards the northwest. A fluorite ore body has a length of 2,900 meters and a thickness ranging from 0.5 to 22.0 meters, with an average thickness of 5.6 meters. And a fluorite ore body extends to a depth of 600 to 800 meters and a vertical depth of 300 to 460 meters (Xu et al., 2009). The fluorite ore in this area includes layered, fine-crystalline, banded, coarse-crystalline, gravel, and sandy types. These can be categorized into quartz-fluorite, quartz-sulfide-fluorite, calcite-quartz-fluorite, and fluorite-quartz styles, with quartz-fluorite style ore being dominant (Xu et al., 2009). Fluorite in this area is commonly off-white, tawny, purple and green (Xu et al., 2009).

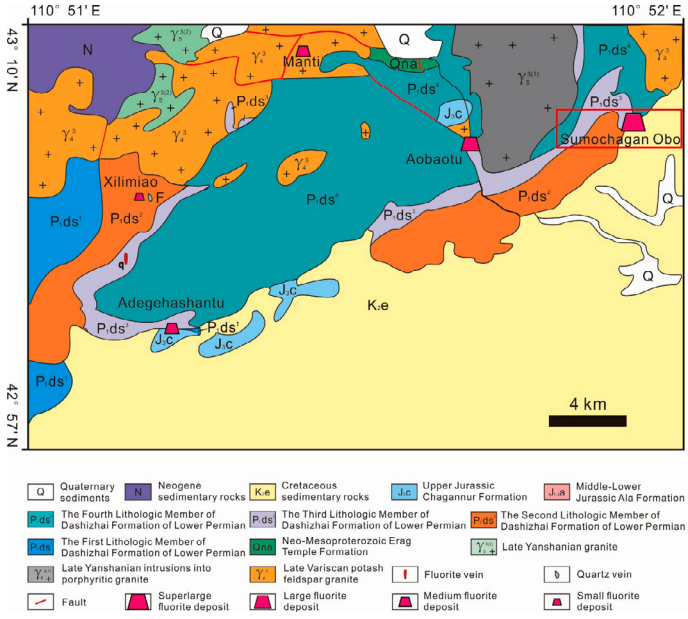

Figure 1. Regional geological map of Siziwangqi showing the distribution of fluorite deposits. (Modified from Bai et al., 2019)

3. Sample Selection and Analytical Methods

The fluorite samples from the Sumochagan Obo deposit, Siziwangqi, Inner Mongolia, can be primarily divided into purple and green series. The green fluorite samples are labeled as NSS1A1, 1A2, 1B1, 1B2, 1C1, 1C2, 1D1, 1D2, 1E1, and 1E2, while the purple fluorite samples are labeled as NSS2A1, 2A2, 2B1, 2B2, 2C1, 2C2, 2D1, and 2D2.

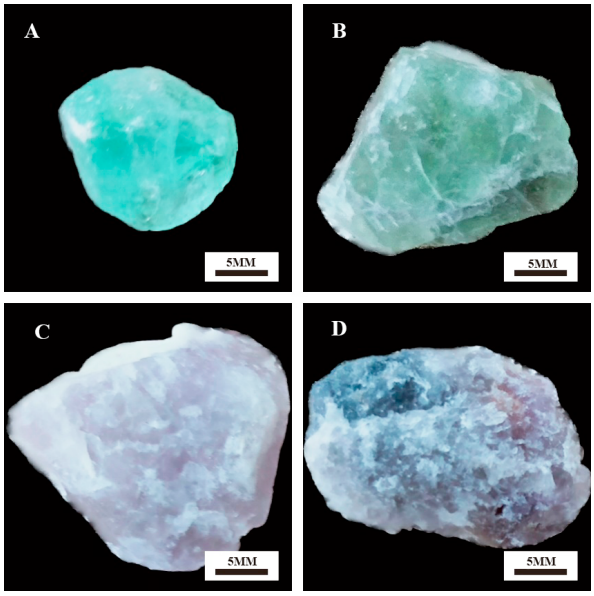

Figure 2. Green and purple fluorite specimens from Sumochagan Obo deposit, Siziwangqi, Inner Mongolia. (a) green fluorite sample 1A1; (b) green fluorite sample 1D2; (c) purple fluorite sample 2A1; (d) purple fluorite sample 2C1.

Luminescence, refractive index, microscopic, and spectroscopic analyses of fluorite samples were conducted at the Gem Laboratory of the School of Gemmology, China University of Geosciences, Beijing. A Diamond View ultraviolet fluorescence spectrometer, produced by the International Institute of Diamond Grading & Research, was used to analyze the luminescence characteristics. A Tensor 27 Fourier-transform infrared spectrometer was employed to obtain the infrared reflection spectrum using the transmission method, with a scanning range of 4000-400 cm^{-1} and a resolution of 4 cm^{-1}. UV-Vis absorption spectroscopy was performed with a GEM-3000 fiber optic spectrometer, using the reflection method and a testing wavelength range of 200-800 nm. Laser Raman spectroscopy was conducted using an HR-Evolution micro-Raman spectrometer produced by HORIBA, Japan. The laser source wavelength was 532 nm, with a Raman laser power of 30-40 mW, a testing range of 100-4000 cm^{-1}, a resolution of 4 cm^{-1}, and a scanning time of 20 seconds.

Geochemical analysis was carried out using an Axios-mAX wavelength dispersive X-ray fluorescence spectrometer and ICP-MS at the Analysis and Testing Center of the Beijing Research Institute of Uranium Geology (BRIUG). The experimental temperature for Axios-mAX analysis was 24°C, with a relative humidity of 24%. ICP-MS trace element composition analysis was performed using an ELEMENT XR plasma mass spectrometer, with an experimental temperature of 22.3°C and a relative humidity of 19%. For fluorite sample preparation, the samples were crushed and ground, and 25-50 mg of each sample was dissolved in hydrofluoric acid and nitric acid. The solution was heated in an oven at 185±5°C for 24 hours, cooled, and then transferred to a hot plate to evaporate the hydrofluoric acid. After dissolution in nitric acid, ICP-MS analysis was conducted.

4. Analytical Results

4.1 Mineralogical Characteristics

The refractive index of fluorite ranges from 1.428 to 1.433, exhibiting a weak to vitreous luster and varying from translucent to opaque. Generally, green fluorite is more transparent than purple fluorite. Under long-wave ultraviolet light, both colors display strong fluorescence, with green fluorite exhibiting stronger fluorescence than purple fluorite. However, under short-wave UV light, the fluorescence is weaker or inert. Under Diamond View, fluorite typically shows blue-white fluorescence. Among them, green fluorite exhibits moderate to strong fluorescence intensity (Figure 3a-c), whereas purple fluorite predominantly demonstrates medium to weak fluorescence with undetectable phosphorescent phenomenon (Figure 3d-f).

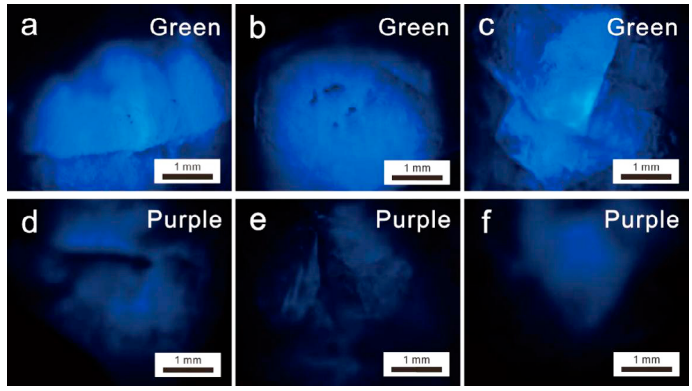

Figure 3. Fluorescence phenomenon of green and purple fluorite. (a-c) moderate to strong fluorescence of green fluorite; (d-f) medium to weak fluorescence of purple fluorite.

Green and purple fluorites have four sets of perfect cleavage, irregular fracture surfaces, and a glassy luster. It is brittle and often associated with quartz. Quartz is mostly colorless to milky white, transparent to translucent, with a vitreous luster and conchoidal fracture surfaces, displaying a greasy luster. Some fluorite samples also contain small amounts of metallic minerals such as chalcopyrite, pyrite, and sphalerite, which exhibit a metallic luster and are opaque. Under magnification, fluorite cleavage and color zoning can be observed in some purple fluorite samples. Petrographic analysis reveals the fluorite contains structural discontinuities (Figure 4a-c, e), hosts solid inclusions (Figure 4d), displays cleavage (Figure 4f), shows oscillatory zoning in purple hues (Figure 4g), and is associated with metallic minerals (Figure 4h, i).

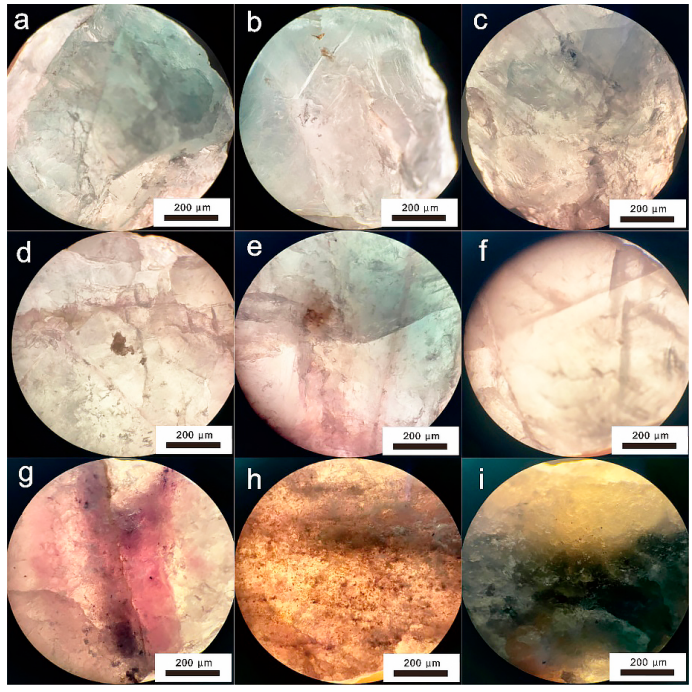

Figure 4. Characteristics of fluorite samples under gem microscope. (a, b, c, e) visible internal fissure; (d) fluid inclusions; (f) clear cleavage; (g) visible purple bands; (h, i) metallic minerals associated with fluorite.

4.2 Spectral Characteristics

4.2.1 Fourier Transform Infrared Spectrum

The green fluorite sample NSS1C2 exhibits absorption peaks at 1097, 1415, 1512, 1643, 2347, 2383, 2852, 2927, and 3384 cm^{-1} (Figure 5a), while the purple fluorite sample NSS2A2 shows absorption peaks at 1082, 1406, 1514, 1643, 2347, 2383, 2852, 2922, and 3384 cm^{-1} (Figure 5b).

Analysis of the absorption peak positions in the infrared spectra indicates the presence of characteristic absorption peaks of CaF_2, CO_3^{2-} stretching vibrations, organic functional group vibrations, and O-H stretching vibrations in both the green fluorite sample NSS1C2 and the purple fluorite sample NSS2A2. The summarized results are presented in Table 1.

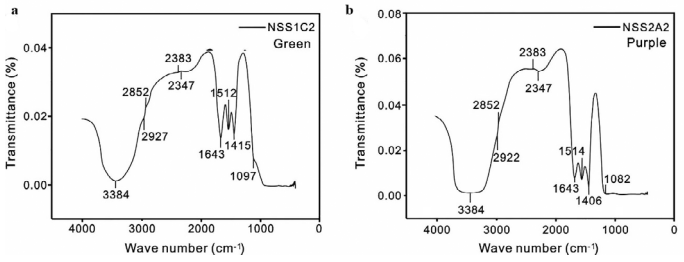

Figure 5. Infrared transmission spectrum of fluorite samples. (a) green fluorite sample 1C2; (b) purple fluorite sample 2A2.

Table 1. Infrared spectrum absorption peaks and peak assignments of fluorite in the Sumochagan Obo area (unit: cm^{-1})

Peak position type	NSS1C2 (Green)	NSS2A2 (Purple)
Characteristic absorption peaks of CaF_2	1097	1082
Telescopic vibration of CO_3^{2-}	1512/1415 1643	1514/1406 1643
Vibration of organic matter groups	2383/2347	2383/2347
O-H telescopic vibration	3384/2927/2852	3384/2922/2852

4.2.2 UV-Visible Absorption Spectrum

Results from the fiber optic spectrometer indicate that sample NSS1A2 exhibits absorption at 223, 264, 275, 363, and 440 nm (Figure 6a), while sample NSS1B2 exhibits absorption at 263, 276, 363, 444, and 587 nm (Figure 6b). Sample NSS2A2 exhibits absorption at 275, 313, 360, and 412 nm (Figure 6c), while sample NSS2B2 exhibits absorption at 261 and 401 nm (Figure 6d).

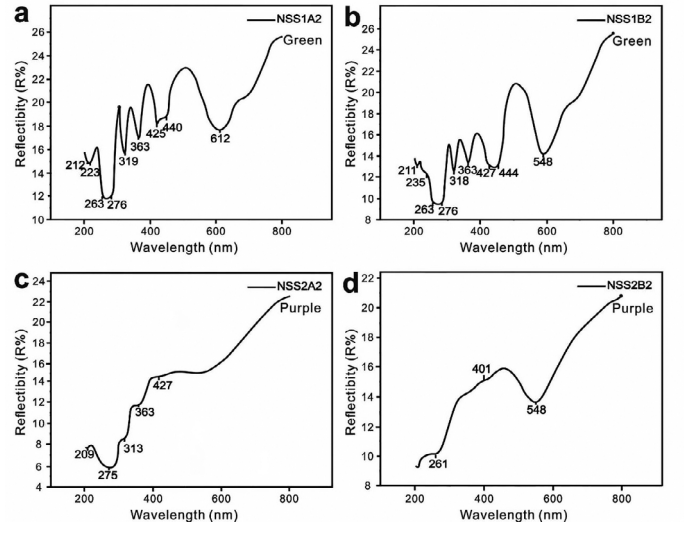

Figure 6. UV absorption spectrum of fluorite samples. (a) green fluorite sample 1A2; (b) green fluorite sample 1B2; (c) purple fluorite sample 2A2; (d) purple fluorite sample 2B2.

4.2.3 Raman Spectrum

Fluorite from Sumochagan Obo in Siziwangqi, Inner Mongolia, exhibits relatively stable Raman absorption peaks at 321 and 323 cm^{-1} (Figure 7). Additionally, the green fluorite samples NSS1B2 and NSS1C2 show absorption peaks around 195, 251, 271, 440, as well as 507, 563, and 646 cm^{-1} (Figure 7a, b). In contrast, the laser Raman spectrum of the purple fluorite samples NSS2C2 and NSS2D2 presents more uniform absorption peaks, with a peak at 321 cm^{-1} and a broad absorption band around 1400-1700 cm^{-1} (Figure 7c, d).

Based on the Raman spectrum data, fluorite samples exhibit four types of characteristic absorption peaks, including those of REE, and peaks of CaF_2, SiO_2, and Fe_3O_4. The summarized data are presented in Table 2. Other peaks are generally caused by impurity elements or inclusions, as some minerals from host rocks mixed in the samples may affect the testing spectrum to some extent.

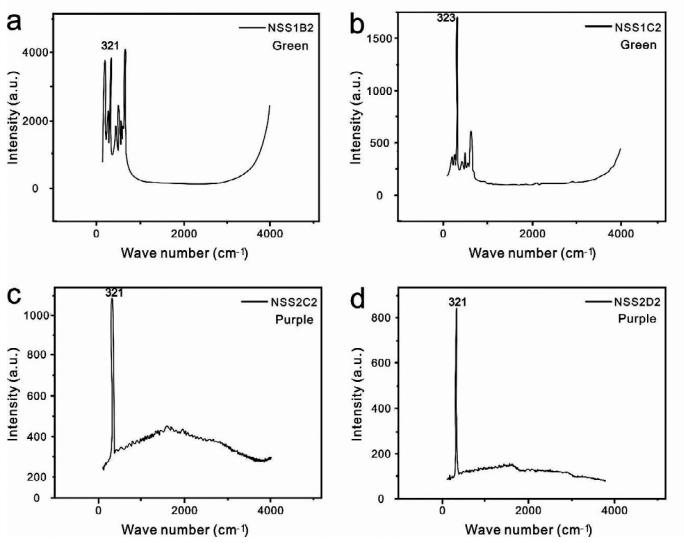

Figure 7. Laser Raman spectrum of fluorite samples. (a) green fluorite sample 1B2; (b) green fluorite sample 1C2; (c) purple fluorite sample 2C2; (d) purple fluorite sample 2D2.

Table 2. Laser Raman spectrum data of green and purple fluorite (unit: cm^{-1})

Characteristic absorption	NSS1B2 (Green)	NSS1C2 (Green)	NSS2C2 (Purple)	NSS2D2 (Purple)
CaF_2	321	323	321	321
SiO_2	195/251/ 271/440	195/251/ 271/440	/	/
Fe_3O_4	507/563/646	507/563/646	/	/
Rare earth peak	/	/	1400~1700	/

4.3 Chemical Composition Analysis

4.3.1 Wavelength Dispersive X-ray Fluorescence Spectrometer

A total of nine samples were tested, including five green fluorite samples (NSS1A1, NSS1B1, NSS1C1, NSS1D1, NSS1E1) and four purple fluorite samples (NSS2A1, NSS2B1, NSS2C1, NSS2D1). The major elemental data of the samples are shown in Table 3. The calcium content in green fluorite is generally higher than in purple fluorite, approximately 66.1%. Fluorite contains 1.69% Si, 0.17% Al, 0.54% Mg, and trace amounts of Fe, Na, K, Mn, Ti, P, and other elements. The loss on ignition of green fluorite is generally lower compared to purple fluorite.

4.3.2 ICP-MS Chemical Composition Analysis

The ICP-MS trace element analytical results are shown in Table 4. The total REE content of the green sample NSS1A1 is anomalously high, while that of the green sample NSS1C1 is anomalously low. However, the values of the other samples are within the normal fluctuation range (Figure 8a). The average total REE content of green fluorite samples is 114.407 ppm, with a median of 92.42 ppm, while the average total REE content of purple fluorite samples is approximately 82.181 ppm, with a median of about 87.55 ppm. Analyzing and comparing the LREE/HREE values of the different fluorites in this area

(Figure 8b), the average LREE/HREE value of green fluorite is 3.547, while that of purple fluorite is 2.086. The LREE/HREE value of green fluorite is significantly higher than that of purple fluorite. Both green and purple fluorites show negative Eu anomalies. The δEu values for green fluorite range from 0.246 to 0.398, with an average of 0.332, while those for purple fluorite range from 0.384 to 0.403, with an average of 0.393. Both green and purple fluorites exhibit positive Ce anomalies. The δCe values for green fluorite range from 0.942 to 1.668, with an average of 1.183, while those for purple fluorite range from 1.217 to 1.679, with an average of 1.426 (Figure 9). The other trace elements in green and purple fluorites are shown in Figure 10. The content of most elements in these samples is generally low, but there are significant differences in the content of some elements between samples. For example, some purple fluorite samples have higher Sr, W, or Co content, while some green fluorite samples show slightly higher Zn or Pb content. The remaining trace element contents are relatively stable.

Table 3. Trace elemental data of green and purple fluorite (unit: Wt%)

Number	Si	Al	MgO	CaO	Na	K	MnO	Ti	P	Loss on ignition*
Detection limits of the elements	0.010	/	/	/	0.010	0.010	0.004	0.006	0.006	/
NSS1A1 (Green)	0.636	0.358	0.060	68.00	0.015	0.009	n.d.	n.d.	0.021	0.49
NSS1B1 (Green)	0.411	0.042	0.058	68.16	0.012	n.d.	n.d.	n.d.	n.d.	0.40
NSS1C1 (Green)	0.509	0.049	0.060	67.82	0.021	n.d.	n.d.	n.d.	n.d.	0.62
NSS1D1 (Green)	n.d.	0.017	0.053	67.88	0.018	n.d.	n.d.	n.d.	0.013	0.63
NSS1E1 (Green)	4.880	0.509	0.219	63.57	0.029	0.017	0.006	0.011	0.023	2.75
NSS2A1 (Purple)	0.057	0.024	0.069	68.68	n.d.	n.d.	n.d.	n.d.	n.d.	1.77
NSS2B1 (Purple)	3.180	0.067	0.054	65.85	n.d.	n.d.	n.d.	n.d.	0.022	1.91
NSS2C1 (Purple)	3.360	0.289	0.124	64.96	0.016	0.036	n.d.	0.011	0.066	2.68
NSS2D1 (Purple)	0.470	0.160	4.180	59.91	0.014	0.023	0.028	0.006	0.115	9.14

Table 4. REE composition and characteristics of green and purple fluorite (ppm)

Number	NSS1A1 (Green)	NSS1B1 (Green)	NSS1C1 (Green)	NSS1D1 (Green)	NSS1E1 (Green)	NSS2A1 (Purple)	NSS2B1 (Purple)	NSS2C1 (Purple)	NSS2D1 (Purple)
La	54.80	28.80	9.050	25.80	23.10	16.10	1.260	34.70	21.00
Ce	35.70	18.30	5.010	17.60	22.80	11.70	1.360	31.20	16.60
Pr	11.30	5.060	1.590	4.990	4.240	3.120	0.360	6.470	4.720
Nd	54.90	22.20	6.140	19.30	18.00	13.10	1.390	25.10	17.70
Sm	12.80	4.600	1.010	3.530	3.100	3.150	0.380	6.470	4.270
Eu	5.660	1.200	0.440	0.990	1.250	1.390	0.150	2.670	1.810
Gd	15.70	5.010	1.200	4.520	3.680	3.750	0.380	7.220	5.150
Tb	3.620	0.850	0.240	0.820	0.780	0.890	0.100	1.510	1.210
Dy	23.70	5.460	1.380	5.210	4.490	6.650	0.650	10.40	9.060
Ho	5.590	1.360	0.330	1.280	1.060	1.510	0.150	2.500	2.390
Er	15.80	4.000	0.990	3.580	2.990	4.520	0.440	7.600	6.480
Tm	2.540	0.660	0.160	0.550	0.500	0.910	0.100	1.260	1.340
Yb	15.50	3.500	1.190	3.740	3.280	6.040	0.740	7.990	8.620
Lu	2.000	0.460	0.170	0.510	0.400	0.810	0.110	0.980	1.110
Y	294.0	71.00	16.50	68.60	52.90	67.30	4.410	111.0	98.80
Li	2.570	1.380	1.420	0.170	10.40	2.450	2.940	5.200	0.821
Be	0.262	0.385	0.501	1.930	4.110	1.820	1.380	7.490	13.40
Sc	0.213	0.138	0.149	0.501	3.330	1.900	0.654	3.290	4.460
V	0.100	0.014	0.123	0.046	2.320	0.335	0.031	2.470	3.740
Cr	0.840	0.473	5.710	1.200	2.530	1.070	2.290	2.600	3.040
Co	24.80	21.20	15.10	11.90	42.90	36.90	56.60	76.90	24.40
Ni	22.80	23.40	22.50	26.10	24.10	20.60	23.40	25.00	21.50
Cu	0.433	0.172	0.121	0.059	2.520	0.230	0.234	1.790	0.674
Zn	2.320	1.270	0.778	1.510	110.0	1.060	1.330	17.10	28.90

(Continued)

Number	NSS1A1 (Green)	NSS1B1 (Green)	NSS1C1 (Green)	NSS1D1 (Green)	NSS1E1 (Green)	NSS2A1 (Purple)	NSS2B1 (Purple)	NSS2C1 (Purple)	NSS2D1 (Purple)
Ga	0.495	0.217	0.120	0.182	1.150	0.816	0.309	1.760	0.682
Rb	0.125	0.036	0.056	0.019	1.240	0.257	0.199	2.640	1.050
Sr	18.60	24.30	57.90	86.00	63.30	109.0	99.70	93.20	201.0
Mo	0.043	<0.002	0.142	0.020	2.020	0.071	0.054	1.020	0.640
Cd	0.112	0.037	0.073	0.091	0.844	0.040	0.073	0.510	1.540
In	0.002	<0.002	0.002	0.002	0.066	<0.002	0.002	0.012	0.006
Sb	0.316	0.312	0.674	0.075	10.90	0.294	3.250	5.390	1.260
Cs	0.041	0.052	0.103	0.005	1.260	0.166	0.248	1.140	0.358
Ba	1.120	1.250	1.120	2.600	18.60	3.380	1.870	19.30	44.90
W	130.0	65.60	73.30	62.40	86.80	73.30	185.0	85.80	48.60
Re	0.003	0.003	<0.002	0.002	0.002	0.002	0.002	<0.002	0.002
Tl	0.005	<0.002	<0.002	<0.002	0.153	0.005	0.007	0.065	0.101
Pb	0.362	0.057	0.173	0.098	106.0	0.666	0.188	3.380	1.290
Bi	0.004	0.005	<0.002	<0.002	1.660	<0.002	0.002	0.090	0.003
Th	0.125	0.135	0.064	0.218	0.331	0.070	0.041	0.444	0.292
U	0.076	0.215	0.101	0.462	3.290	0.256	0.245	2.160	6.230
Nb	0.027	0.007	0.004	0.010	0.046	0.027	0.020	0.086	0.062
Ta	0.100	0.027	0.017	0.020	0.035	0.029	0.039	0.027	0.030
Zr	0.142	0.084	0.074	0.224	1.070	0.525	0.328	1.300	1.850
Hf	0.248	0.021	0.011	0.041	0.064	0.074	0.021	0.123	0.106
Sn	0.056	0.025	0.022	0.020	0.346	0.092	0.087	0.341	0.169
ΣREE	259.6	101.5	28.90	92.42	89.67	73.64	7.570	146.1	101.5
ΣLREE	175.2	80.16	23.24	72.21	72.49	48.56	4.900	106.6	66.10
ΣHREE	84.45	21.30	5.660	20.21	17.18	25.08	2.670	39.46	35.36
ΣLREE/ ΣHREE	2.074	3.763	4.106	3.573	4.219	1.936	1.835	2.702	1.869
La/Lu	27.40	62.61	53.24	50.59	57.75	19.88	11.45	35.41	18.92
δEu	0.397	0.250	0.398	0.246	0.369	0.403	0.395	0.390	0.384
δCe	1.080	1.081	0.942	1.143	1.668	1.217	1.679	1.516	1.291

Note: $\delta Eu=2Eu_N/(Sm_N+Gd_N)$, $\delta Ce=2Ce_N/(La_N+Pr_N)$.

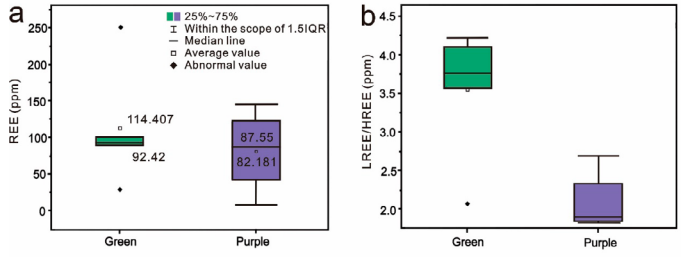

Figure 8. (a) the box plots of total REE concentrations for green and purple fluorite samples; (b) the box plots of LREE/HREE ratios for green and purple fluorite samples.

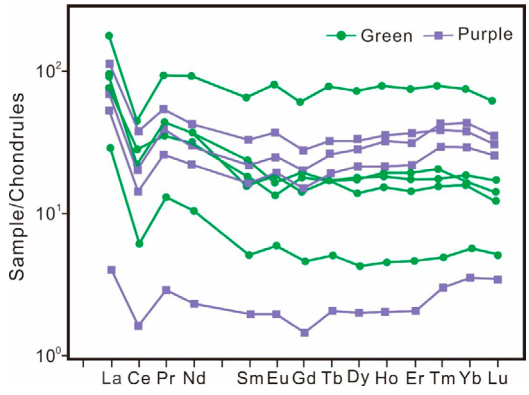

Figure 9. Distribution of REE chondrite-normalized patterns for green and purple fluorite samples.

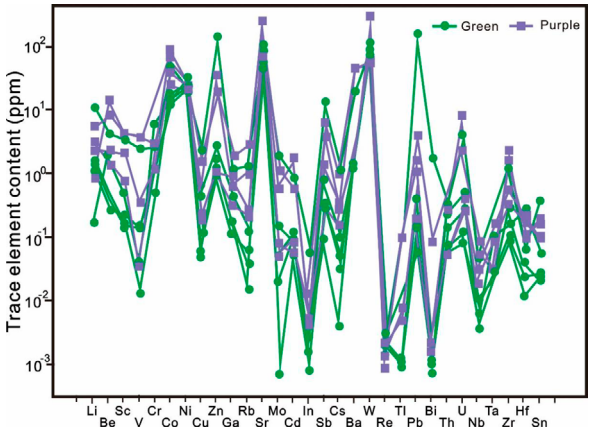

Figure 10. Spider diagrams of trace elements for green and purple fluorite samples.

5. Discussion

5.1 Coloration Mechanism

Previous studies have identified three main coloration mechanisms in fluorite: impurity-related color centers, divalent rare earth ion coloration, and coloration by metal calcium colloids. These mechanisms have been widely applied in investigating various fluorite coloration phenomena (Table 5; Bill and Galas, 1978).

Impurity-Related Color Centers: Impurity-related color centers in fluorite arise because CaF_2, the primary component of fluorite, typically contains cationic impurities. At temperatures below 100 °C, oxygen ions can be introduced into the crystal lattice through hydrolysis during hydrothermal activities (Bontinck, 1958). At high temperatures, oxygen ions combine with cationic impurities to form localized molecular structures. When irradiated with ionizing radiation at room temperature, crystals containing impurities exhibit many optical absorption bands associated with these impurities (Bill and Galas, 1978). These impurity-induced color centers can be categorized into three types: (a) Rare-earth element and F Centers. Studies on naturally colored fluorites suggest that Y-complexed F centers generally result in blue coloration. These color centers exhibit C_{3v} point symmetry along the [111] axis and are associated with Y^{3+} ions related to F^- vacancies. Linear dichroism experiments (Staebler and Schnatterly, 1971) and research by Alig (1971) indicate that the three low-energy bands polarize in increasing order of energy, consistent with transitions from the $1A_1$ ground state orbital to the 1E, $2A_1$, and 2E levels. This polarization arises from the overlap of the F center wavefunction with the 4d and 5s orbitals of Y^{3+} (Staebler and Schnatterly, 1971). F centers in the UV-visible absorption spectrum show weak supplementary lines at 580/400/335/224 nm, and at 250/310/720 nm for Y and F centers. Additional bands near 300 nm, a central absorption band at 485 nm, and peaks at 580/714 nm are also observed for Y, Ce, and F centers (Bill and Galas, 1978). The 223 nm absorption peak in sample NSS1A2 may be attributed to the bluish tint of fluorite. (b) YO_2 Centers. These centers impart a rose color to fluorite and consist of three nearest neighboring F centers within the fluorite lattice. YO_2 centers can be generated in CaF_2 crystals doped with YF_3 that have undergone hydrolysis upon exposure to X-rays. Research using EPR and ENDOR techniques indicates that YO_2 centers are composed of O_2^{3-} ions and are stabilized by Y^{3+} ions (Bill and Galas, 1978). In the UV-visible absorption spectrum, the absorption peaks are primarily observed at 485/225/260/270/365 nm (Bill and Galas, 1978). UV-visible absorption spectra of samples NSS2A2 and NSS2B2 exhibit absorption peaks at 275/261 nm, indicating the presence of YO_2 color centers. (c) O^{2-} Ion Replacement. O^{2-} ions replace two nearest neighboring F^- ions with the directions of the two outer oxygen nuclei parallel to the tetragonal crystal axis. The molecular ions undergo vibrational motion, with charge compensation primarily carried out by substituted Na^+ ions. This is manifested by a broad absorption band at 434 nm and an absorption peak at 230 nm (Bill and Galas, 1978).

Divalent Rare Earth Ion Coloration. The primary color centers of rare earth ions in fluorite are typically Sm^{2+}, which generally imparts a green color to the mineral. Previous studies suggested that the reduction of radiation-induced trivalent rare earth ions can only occur at sites located in the cubic position, which possess remote charge compensation. Hayes and Twidell (1961) proposed the repulsive Coulomb effect of negative charge compensators, which impedes the capture of electrons by adjacent rare earth ions. Consequently, divalent rare earth ions can only occupy the cubic position. During the transition from trivalent to divalent rare earth ions, the energy of the 5d orbitals decreases relative to the 4f orbitals. The broadening of the absorption spectrum arises from the interaction between the unshielded 5d electrons and lattice vibrations, with the intensity of the allowed transitions contrasting with the energy bands formed by forbidden internal transitions (Bill and Galas, 1978). The absorption peaks of Sm^{2+} color centers are located at 690/611/440 nm, with a broad absorption band at 422 nm and in the ultraviolet region at 360/335/305/279 nm, possibly interfered by strong defect absorption. Additionally, Eu^{2+} may produce an absorption peak around 413 nm. The UV-visible spectra of green fluorite samples NSS1A2, NSS1B2, and NSS1C2 exhibit absorption peaks at 693/440/360/276 nm, potentially attributed to Sm^{2+} color centers, with REE content of approximately 3.31 ppm.

Metal Calcium Colloids. High-radiation environments can impart color to colorless fluorite, resulting in non-uniform and highly stable colors (Liu et al., 1983). Heating in the vapor of metallic calcium can cause calcium atoms to enter the fluorite structure in the form of colloidal particles, giving colorless fluorite a purple hue (Li et al., 1985). The formation of colloidal calcium primarily relies on crystal defects in fluorite to provide sites (Li et al., 1985). This is manifested by absorption peaks around 560-580 nm in the UV-visible spectrum. Sample NSS1B2 exhibits absorption at 587 nm, and sample NSS1C2 shows absorption at 591 nm, suggesting that this may be attributed to colloidal calcium color centers. XRF testing indicates higher calcium content in green fluorite, suggesting that in some cases, calcium in Sumochagan Obo fluorite may exist in the form of colloidal calcium within crystal defects, thereby causing coloration.

In summary, the coloration mechanisms in fluorite from the Sumochagan Obo deposit vary among samples. The primary reasons for the green coloration are rare earth with F centers, Sm^{2+}, and colloidal calcium color centers, while the YO_2 center is responsible for the purple coloration of fluorite (Table 5).

Table 5. Characteristic absorption peaks of fluorite from the Sumochagan Obo deposit

Absorption peak position	NSS1A2 (Green)	NSS1B2 (Green)	NSS1C2 (Green)	NSS2A2 (Purple)	NSS2B2 (Purple)	References
Color center caused by impurities	223/264/275/363	263/276/363	263/273/364	275 313	261 401	(Bill and Galas, 1978)
Color center of rare earth ions	275/363/440	276/363/444	364/427/693	275/360/412	/	(Bill and Galas, 1978)
Calcium colloid color center	/	587	591	/	/	(Bill and Galas, 1978)

5.2 Ore-forming fluid source

The atomic ratio of Tb/Ca reflects the chemical environment of fluorite crystallization and holds genetic significance, while the Tb/La atomic ratio indicates the degree of REE fractionation in fluids and the alteration effects of ore-forming fluids during mineralization. A bivariate plot of Tb/La against Tb/Ca can be used to determine the genetic types of fluorites and ascertain whether ore-forming fluids have undergone hydrothermal reactions with host rocks (Schneider et al., 1975; Möller, 1976). Previous studies have used Tb/Ca-Tb/La plots to analyze multiple fluorite samples worldwide, classifying deposit genesis into pegmatite, hydrothermal, and sedimentary types (Möller and Morteani, 1983; Bau and Dulski, 1995).

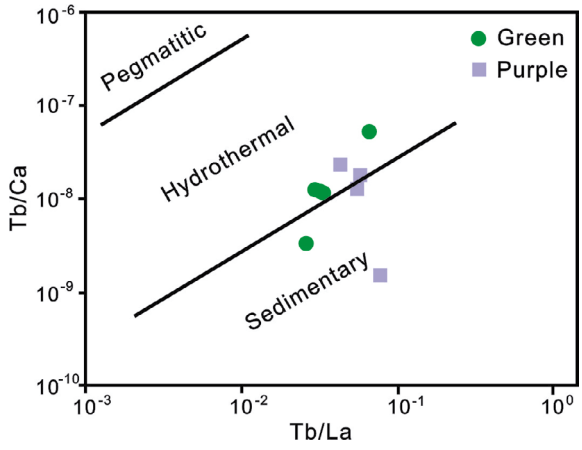

Figure 11. Diagram of Tb/Ca-Tb/La for green and purple fluorite.

Fluorite in magmatic-hydrothermal deposits typically occurs with other major minerals (Wang et al., 2019; Li, 2021). In deposits where meteoric water is the primary ore-forming fluid, fluorite is the main mineral (Suo et al., 2020; Wang et al., 2020). The Tb/Ca-Tb/La plot of fluorite from Sumochagan Obo, Siziwangqi, Inner Mongolia (Figure 11), suggests a predominantly hydrothermal origin, consistent with geological and petrological observations. This is similar to findings in Yangshan in western Henan (Feng et al., 2020), Checun in Henan (Dong et al., 2020), Huangbi in Jiangxi (Huang et al., 2018), Pucheng in Fujian (Zhu et al., 2021), and Xiaodongzi in Butuo (Luo et al., 2020). Previous studies suggest that in the Tb/Ca-Tb/La plot, fluorite samples closer to the sedimentary area tend to extract more Ca elements from host rocks during formation, indicating a higher degree of water-rock interaction (Dill et al., 1986). The purple fluorite samples from this mining area, compared to the green fluorite samples, are closer to the sedimentary zone, suggesting a potentially higher degree of water-rock interaction during their precipitation.

By summarizing the characteristics of REE in different fluorite deposits and the sources of ore-forming fluids from previous studies, it can be inferred that fluorite deposits primarily sourced from magmatic-hydrothermal fluids generally have higher ∑REE content compared to those mainly sourced from meteoric water. The REE content of fluorite from Sumochagan Obo is similar to fluorite sourced from a mixture of magmatic-hydrothermal and meteoric water (Table 6). Additionally, K-Ar ages of hydrothermal sericite and illite in fluorite deposits are 141.5±1.2 Ma and 137.6±1.1 Ma, respectively, which are close to the ages of zircon in fine-grained granite veins with fluorite mineralization within the regional Weijing granite (SHRIMP U-Pb, 137±2 Ma; Xu et al., 2009). This indicates that the mineralization age of fluorite aligns with the timing of granitic magmatic activity, suggesting that granite-related hydrothermal fluids may be a potential source of ore-forming fluids.

6. Conclusions

The analysis of the UV-visible absorption spectra of fluorite samples from the Sumochagan Obo area, Siziwangqi, Inner Mongolia, suggests that YO_2 centers may contribute to the purple coloration of fluorite in this region, as indicated by the 276/261 nm absorption peaks observed in purple samples. The green coloration of fluorite is primarily attributed to the presence of REE, F centers, and Sm^{2+}. Additionally, some Ca in the fluorite may exist as colloidal calcium within crystal defects, contributing to its coloration. In the UV-visible absorption spectra, green samples exhibit a 223 nm absorption peak characteristic of Y and F centers, peaks at 693/440/360/276 nm due to Sm^{2+}, and absorption at 587/591 nm attributed to calcium colloid color centers.

The geological characteristics of fluorite in this mining area, along with the Tb/Ca-Tb/La plot, indicate a predominantly magmatic-hydrothermal origin. The geochemical characteristics of REE in fluorite and the sources of ore-forming fluids resemble those of fluorite deposits formed through a mixture of magmatic-hydrothermal and meteoric water. Water-rock interaction is identified as the predominant mechanism for fluorite precipitation.

Acknowledgements

This work was financially supported by the "Deep-time Digital Earth" Science and Technology Leading Talents Team Funds for the Central Universities, China University of Geosciences (Beijing) (Grant number: 2652023001), the 111 Project of the Ministry of Science and Technology, China (Grant No. BP0719021), and MOST Special Fund from the State Key Laboratory of Geological Processes and Mineral Resources, China University of Geosciences (Grant No. MSFGPMR201804). The Professional Committee of Tectonophysicochemistry, Chinese Geophysical Society provided theoretical support.

References

Alig, R. C. (1971). Theory of photochromic centers in CaF_2. *Physical Review, B3*, 536-545. https://doi.org/10.1103/PhysRevB.3.536

Alipour, S., Abedini, A. & Talaei, B. (2014). Geochemical characteristics of the Qahr-Abad fluorite deposit, southeast of Saqqez, western Iran. Arabian Journal of Geosciences, 8 (9), 7309-7320. https://doi.org/10.1007/s12517-014-1747-6

Table 6. REE characteristics and ore-forming fluid sources of fluorite in different deposits

Deposit	∑REE ($\times10^{-6}$)	Fluid Source	References
Baiyun Ebaoxi Mining Area in Inner Mongolia	8841 ~ 20122	Predominantly magmatic water	(Liu et al., 2022)
Nanlishu in Jilin	8.070 ~ 27.23	predominantly meteoric water	(Ye and Bai, 2022)
Kentian in Ningdu, Jiangxi	34.11 ~ 78.12	predominantly meteoric water	(You et al., 2022)
Shuitou in Inner Mongolia	1.120 ~ 64.50	predominantly meteoric water	(Pei et al., 2017)
Xiaobeigou in Inner Mongolia	3.840 ~ 30.21	predominantly meteoric water	(Pei et al., 2019)
Gaoling in Southwest Guizhou	11.40 ~ 105.0	Magmatic and meteoric water	(Jin et al., 2018)
Tiantai Basin in Zhejiang	69.41 ~ 142.67	Magmatic and meteoric water	(Zou et al., 2014)
Lishan in Hunan	3.519 ~ 204.9	Magmatic and meteoric water	(Chen et al., 2023)
Sumochagan Obo in Siziwangqi, Inner Mongolia	7.556 ~ 259.61	Magmatic and meteoric water	This paper

Aoki, T., Garvie, L. A. J. & Rez, P. (2015). Observation of color center peaks in calcium fluoride. Ultramicroscopy, 153, 40-44. https://doi.org/10.1016/j.ultramic.2015.02.007

Azizi, R. M., Abedini, A., Alipour, S. & Bagheri, H. (2018). The Laal-Kan fluorite deposit, Zanjan Province, NW Iran: Constraints on REE geochemistry and fluid inclusions. Arabian Journal of Geosciences, 11(22), 719. https://doi.org/10.1007/s12517-018-4055-8

Azizi, R. M., Abedini, A. & Alipour, S. (2020). Application of lanthanides tetrad effect as a geochemical indicator to identify fluorite generations: A case study from the Laal-Kan fluorite deposit, NW Iran. Comptes Rendus Geoscience, 352(1), 43-58. https://doi.org/10.5802/crgeos.2

Bai, Y., Wang, Z. G., Wang, G. H., Zhu, L., Yao, F. S. & Yan, G. Q. (2019). Metallogenic model of fluorite deposits in Siziwangqi, Inner Mongolia: implications for the prospecting of volcanic type uranium deposits. Metal Mine, 4, 121-128. (in Chinese with English Abstract) https://doi.org/10.19614/j.cnki.jsks.201904024

Barnes, H. (2015). Hydrothermal processes: The development of geochemical concepts in the latter half of the twentieth century. Geochemical Perspectives, 4(1), 1-93. https://doi.org/10.7185/geochempersp.4.1

Bau, M. & Dulski, P. (1995). Comparative-study of Yttrium and rare-earth element behaviors in fluorine-rich hydrothermal fluids. Contributions to Mineralogy and Petrology, 119(2), 213-223. https://doi.org/10.1007/BF00307282

Bill, H. & Calas, G. (1978). Color centers, associated rare-earth ions and the origin of coloration in natural fluorites. Physics and Chemistry of Minerals, 3(2) ,117-131. https://doi.org/10.1007/BF00308116

Bontinck, W. (1958). The hydrolysis of solid CaF_2. Physica, 24(6-10), 650-658. https://doi.org/10.1016/s0031-8914(58)80079-8

Boynton, W. V. & Wark, D. A. (1984). Trace element abundances in rim layers of an Allende type a coarse-grained, Ca, Al-rich inclusion. Meteoritics, 19(4), 195-197. https://www.researchgate.net/publication/234505003

Chen, Z. Y., Ye, X. M., Zhang, L., Shi, S. Y., Xiong, Y. Q., Bai, F., Yu, T. W. & Shen, G. W. (2023). REE geochemical characteristics of hydrothermal fluorite, Lishan copper-lead-zinc polymetallic deposit, northeastern Hunan Province and its indicative significance. Acta Petrologica Sinica, 39(02), 532-546. (in Chinese with English Abstract) https://doi.org/10.18654/1000-0569/2023.02.15

Dill, H. G., Möller, P. & Dulski, P. (1986). Fluorite mineralization and REE patterns in vein-type deposits from the N Bavarian Basement (Germany). Neues Jahrbuch für Mineralogie-Abhandlungen, 154(2), 141-151. https://www.researchgate.net/publication/265594809

Dill, H. G. & Weber, B. (2010). Variation of color, structure and morphology of fluorite and the origin of the hydrothermal F-Ba deposits at Nabburg-Wolsendorf, SE Germany. Neues Jahrbuch für Mineralogie-Abhandlungen, 187, 113-132. https://doi.org/10.1127/0077-7757/2010/0169

Ding, Z. J., Yao, S. Z., Liu, C. Q., Zhou, Z. G. & Yang, M. G. (2003). The characteristics of exhalation-sedimentary deposit of Donggouba polymetal deposit: Evidence from ore's REE composition. Acta Petrologica Sinica, 19(4), 792-798. (in Chinese with English Abstract) https://doi.org/10.1029/90JC01868

Dong, W. C., Pang, X. C., Si, Y. Y., Liang, Z. & Li, W. M. (2020). REE geological characteristics of Checun fluorite deposit in Song County, Henan province. Journal of the Chinese Society of Rare Earths, 38(05), 706-714. (in Chinese with English Abstract) https://doi.org/10.11785/S1000-4343.20200516

Feng, S. P., Wang, J. H., Liu, Y. W., Liang, X. H., Huang, L., Zhang, Z. H. & Xiao, H. Z. (2020). Geochemical characteristics, and indicative significance of rare-earth elements in Yangshan fluorite deposit in western Henan province. Chinese Rare Earths, 41(05), 50-58. (in Chinese with English Abstract) https://doi.org/10.16533/j.cnki.15-1099/tf.20200032

Gaft, M., Waychunas, G. A., Rossman, G. R., Nagli, L., Panczer, G., Cheskis, D. & Raichlin, Y. (2020). Red photoluminescence and purple color of naturally irradiated fluorite. Physics and Chemistry of Minerals, 47(11), 45-56. https://doi.org/10.1007/s00269-020-01116-4

Haschke, S., Gutzmer, J., Wohlgemuth-Ueberwasser, C. C., Kraemer, D. & Burisch, M. (2021). The Niederschlag fluorite-(barite) deposit, Erzgebirge/Germany: A fluid inclusion and trace element study. Mineralium Deposita, 56(6), 1-16. https://doi.org/10.1007/S00126-020-01035-Y

Hayes, W. & Twidell, J. W. (1961). Paramagnetic resonance of X-irradiated CaF_2: Tm and CaF_2: Yb. The Journal of Chemical Physics, 35(4), 1521-1522. https://doi.org/10.1063/1.1732094

Huang, C. J., Wang, J. Z. & Li, Z. Q. (2015). REE geochemistry of fluorite from Lala IOCG deposit, SW margin of Yangtze Block. Acta Mineralogica Sinica, 35(1), 95-102. (in Chinese with English Abstract) https://doi.org/10.16461/j.cnki.1000-4734.2015.01.014

Huang, H. X., Luo, P., Chang, S. M., Zhang, J. & Wang, C. H. (2018). Characteristics of rare earth elements and the source of mineralization of fluorite deposit in Huangbi, Jiangxi Province. Mineral Resources and Geology, 32(04), 641-646+654. (in Chinese with English Abstract) https://doi.org/10.3969/j.issn.1001-5663.2018.04.006

Jin, S. R., Chen, J., Dai, D. R., Yang, D. Z., Zhou, J. X. & He, X. H. (2018). Geochemical characteristics of trace and rare Earth elements in the Gaoling fluorite deposit, southwestern Guizhou. Acta Mineralogica Sinica, 38(06), 684-692. (in Chinese with English Abstract) https://doi.org/10.16461/j.cnki.1000-4734.2018.38.244

Li, X. A., Liu, T. G. & Zhao, Y. L. (1985). Study on the dyeing mechanism of fluorite in Bayan Obo. Acta Mineralogica Sinica, 02, 164-168+196. (in Chinese with English Abstract) https://doi.org/10.16461/j.cnki.1000-4734.1985.02.011

Li, Z. J. (2021). Geological characteristics and genesis of Huitan fluorite deposit in Jianyang, city, Fujian province. Geology of Fujian, 40(01), 13-23. (in Chinese with English Abstract) https://doi.org/10.3969/j.issn.1001-3970.2021.01.002

Liu, B., Wu, Q. H., Li, H., Wu, J. H., Cao, J. Y., Jiang, J. B. & Liang, W. (2020). Fault-controlled fluid evolution in the Xitian W–Sn–Pb–Zn–fluorite mineralization system (South China): Insights from fluorite texture, geochemistry and geochronology. Ore Geology Reviews, 116, 103233. https://doi.org/10.1016/j.oregeorev.2019.103233

Liu, S. H., Wang, C. L., Liu, D. H., Wang, J., Ke, C. H., You, C. & Zhou, B. W. (2022). Geochemical characteristics of rare Earth elements of associated fluorite deposits in the Bayan Obo area and their implications. Acta Petrologica et Mineralogica, 41(05), 903-915. (in Chinese with English Abstract) https://doi.org/10.3969/j.issn.1000-6524.2022.05.004

Liu, T. G., Zhao, Y. L. & Li, X. A. (1983). Preliminary study on radiation damage and fluorite color. Acta Mineralogica Sinica, 04, 300-303+326. (in Chinese with English Abstract) https://doi.org/10.16461/j.cnki.1000-4734.1983.04.011

Luo, L. P., Tan, H. Q., Hu, J. L., Xie, H. F. & Zhang, W. (2020). REE geochemistry of the Xiaodongzi fluorite deposit in Butuo. Acta Geologica Sichuan, 40(01), 45-50. (in Chinese with English Abstract) https://doi.org/10.3969/i.issn.1006-0995.2020.01.010

Möller, P., Parekh, P. P. & Schneider, H. J. (1976). The application of Tb/Ca-Tb/La abundance ratios to problems of fluorspar genesis. Mineralium Deposita, 11(1), 111-116. https://doi.org/10.1007/BF00203098

Möller, P. & Morteani, G. (1983). On the geochemical fractionation of rare earth elements during the formation of Ca-minerals and its application to problems of the genesis of ore deposits. Theophrastus Publications. https://www.researchgate.net/publication/279907357

Pei, Q. M., Zhang, S. T., Santosh, M., Cao, H. W., Zhang, W., Hu, X. K. & Wang, L. (2017). Geochronology, geochemistry, fluid inclusion and C, O and Hf isotope compositions of the Shuitou fluorite deposit, Inner Mongolia, China. Ore Geology Reviews, 83, 174-190. https://doi.org/10.1016/j.oregeorev.2016.12.022

Pei, Q. M., Zhang, S. T., Hayashi, K. I., Wang, L., Cao, H. W., Zhao, Y., Hu, X. K., Song, K. R. & Chao, W. W. (2019). Nature and genesis of the Xiaobei-

gou fluorite deposit, Inner Mongolia, Northeast China: Evidence from fluid inclusions and stable isotopes. Resource Geology, 69(2), 148-166. https://doi.org/10.1111/rge.12191

Redina, A. A., Nikolenko, A. M., Doroshkevich, A. G., Prokopyev, I. R., Wohlgemuth-Ueberwasser, C. & Vladykin, N. V. (2020). Conditions for the crystallization of fluorite in the Mushgai-Khudag complex (southern Mongolia): Evidence from trace element geochemistry and fluid inclusions. Geochemistry, 80(4), 125666. https://doi.org/10.1016/j.chemer.2020.125666

Richardson, C. K. & Holland, H. D. (1979). Fluorite deposition in hydrothermal systems. Geochimica et Cosmochimica Acta, 43(8), 1327-1335. https://doi.org/10.1016/0016-7037(79)90122-4

Schneider, H. J., Möller, P. & Parekh, P. P. (1975). Rare earth element distribution in fluorites and carbonate sediments of the east Alpine mid-Triassic sequences in the Nordliche Kalkalpen. Mineralium Deposita, 10(4), 330-344. https://doi.org/10.1007/BF00207892

Schwinn, G. & Markl, G. (2005). REE systematics in hydrothermal fluorite. Chemical Geology, 216(3-4), 225-248. https://doi.org/10.1016/j.chemgeo.2004.11.012

Shannan, R. D. (1976). Revised effective ionic radii and systematic studies of interatomic distances in halides and chalcogenides. Acta Crystallographica Section A, 32(5), 751-767. https://doi.org/10.1107/S0567739476001551

Staebler, D. L. & Schnatterly, S. E. (1971). Optical studies of a photochromic color center in rare-earth doped CaF_2. Physical Review, B3, 516-526. https://doi.org/10.1103/PhysRevB.3.516

Sun, H. R., Huang, Z. L. & Zhou, J. X. (2014). Rare earth element geochemistry of fluorite in hydrothermal deposits and its geological significance. Acta Petrologica et Mineralogica, 33(01), 185-193. (in Chinese with English Abstract) https://doi.org/10.3969/j.issn.1000-6524.2014.01.014

Sun, X., Yang, Z. R., Liu, J. D., Wang, Y. C., Wang, W. W. & Xu, D. D. (2008). REE geochemistry of fluorite from Yixian fluorite deposit and its geological implications. Mineral Deposits, 05, 579-586. (in Chinese with English Abstract) https://doi.org/10.3969/j.issn.0258-7106.2008.05.004

Sun, X., Yang, Z. R., Wang, Y. C., Liu, J. D., Wang, W. W. & Xu, D. D. (2009). Sr isotopic composition and genesis in Yixian fluorite deposit. Bulletin of Geological Science and Technology, 28(01), 82-86. (in Chinese with English Abstract) https://doi.org/10.3969/j.issn.1000-7849.2009.01.013

Sun, X., Deng, J., Yang, L. Q., Wang, Q. F., Yang, Z. R., Gong, Q. J. & Wang, C. M. (2010). Ree and Sr-Nd isotope geochemistry for Yixian fluorite deposit, western Liaoning Province, China, and its geological implications. Journal of Earth Science, 21(2), 227-235. https://doi.org/10.1007/s12583-010-0020-5

Suo, Z. L., Wang, S., Yu, Z. H., Li, Y. Q., Yuan, Y. W. & Wang, X. L. (2020). Hydrogen, oxygen, lead and sulfur isotopic and geochemical characteristics of fluorite deposits in the North Dabie Mountains. Mineral Resources and Geology, 34(01), 41-47. (in Chinese with English Abstract) https://doi.org/10.19856/j.cnki.issn.1001-5663.2020.01.006

Wang, L. L., Ni, P., Dai, B. Z., Li, W. S., Pan, J. Y., Cui, J. M. & Gao, Y. (2020). Fluid inclusion study of the ore-bearing stockwork greisen at Shizhuyuan W-Sn-Mo-Bi deposit, Hunan. Journal of Nanjing University (Natural Science), 56(05), 653-665. (in Chinese with English Abstract) https://doi.org/10.13232/j.cnki.jnju.2020.05.005

Wang, X. L., Wang, S., Yuan, Y. W. & Li, Y. Q. (2019). Characteristics of geological and metallogenic fluids on Bancang fluorite mine in Dawu, Hubei. Mineral Exploration, 10(09), 2256-2260. (in Chinese with English Abstract) https://doi.org/10.3969/j.issn.1674-7801.2019.09.016

Xu, D. Q., Nie, F. J., Qian, M. P., Liu, Y., Yun, F. & Zhang, W. Y. (2009). Rare Earth element geochemistry of the Sumochagan Obo super-large fluorite deposit and its genetic significance. Mineral Deposits, 28(01), 29-41. (in Chinese with English Abstract) https://doi.org/10.3969/j.issn.0258-7106.2009.01.003

Ye, X. M. & Bai, F. (2022). Spectral characteristics, rare earth elements, and ore-forming fluid constrains on the origin of fluorite deposit in Nanlishu, Jilin Province, China. Minerals, 12(10), 1195. https://doi.org/10.3390/MIN12101195

You, C., Wang, C. L., Liu, D. H., Yu, X. C., Yan, K., Liu, S. H. & Zhou, B. W. (2022). Geochemical characteristics of rare Earth elements of the Kantian fluorite deposit in Ningdu, Jiangxi Province and its indication. Acta Geoscientica Sinica, 43(03), 359-370. (in Chinese with English Abstract) https://doi.org/10.3975/cagsb.2022.040101

Yu, C. F., Pan, W., Zhang, Y. T., Li, H. B., Tian, Q. L. (2018). Application of remote sensing technology to uranium exploration in Sumoqagan Obo area, Inner Mongolia. Uranium Geology, 34(06), 372-378. (in Chinese with English Abstract) https://doi.org/10.3969/j.issn.1000-0658.2018.06.008

Zeng, Z. F., Cao, H. W., Gao, F., Gao, Y. Z., Zou, H. & Li, D. (2013). Fluid inclusion study of fluorite deposits in Linxi region, Inner Mongolia. Geochimica, 42(01), 73-81. (in Chinese with English Abstract) https://doi.org/10.19700/j.0379-1726.2013.01.007

Zhang, J. J., Hu, D. M. & Chen, X. L. (2021). Geological characteristics of fluorite deposit in Yangshan area of Luanchuan County, Henan Province and its prospecting prospect. Shanxi Metallurgy, 44(01), 93-95. (in Chinese with English Abstract) https://doi.org/10.16525/j.cnki.cn14-1167/tf.2021.01.31

Zhang, Y. T., Pan, W. & Yu, C. F. (2019). Application of World View-3 image in uranium exploration in Sumochagan Aobao area, Inner Mongolia. Uranium Geology, 35(02), 114-121. (in Chinese with English Abstract) https://doi.org/10.3969/j.issn.1000-0658.2019.02.008

Zhao, P., Zheng, H. Y. & Zhang, X. (2020). Present situation and development suggestions of fluorite industry resources in China. Geology of Chemical Minerals, 42(02), 178-183. (in Chinese with English Abstract) https://doi.org/10.3969/j.issn.1006-5296.2020.02.014

Zhou, B. W., Wang, C. L., You, C., Liu, D. H., Liu, S. H., Yu, X. C., Yan, K., Liu, X. & Liu, Y. T. (2022). Geochemical characteristics of trace elements and REE in Zhangcuo fluorite deposit in Shaowu area, Fujian Province. Acta Geoscientica Sinica, 43(03), 393-403. (in Chinese with English Abstract) https://doi.org/10.3975/cagsb.2022.042701

Zhu, L. G., Jin, S., Wang, C. L., Shang, P. Q., Gao, L. Y. & Wang, Z. B. (2021). Geochemistry characteristic and genesis of surrounding rock and ore Pucheng fluorite deposit district, Fujian province. Acta Petrologica et Mineralogica, 40(05), 923-938. (in Chinese with English Abstract) https://doi.org/10.3969/j.issn.1000-6524.2021.05.005

Zou, H., Fang, Y. & Chen, H. M. (2014). Geochemical characteristics and genesis of rare Earth elements in the Xiachen fluorite deposit, Tiantai Basin, Zhejiang Province. Geology in China, 41(04), 1375-1386. (in Chinese with English Abstract) https://doi.org/10.3969/j.issn.1000-3657.2014.04.027